Dalton Transactions

PAPER

View Article Online
View Journal

Cite this: DOI: 10.1039/c4dt03272a

Zinc oxide nanocrystal quenching of emission from electron-rich ruthenium-bipyridine complexes†

Ryan J. Hue, Rajan Vatassery, Kent R. Mann and Wayne L. Gladfelter*

Received 23rd October 2014,
Accepted 28th January 2015

DOI: 10.1039/c4dt03272a

www.rsc.org/dalton

A series of heteroleptic bipyridine ruthenium complexes were prepared using known synthetic methods. Each compound incorporated one electron withdrawing 4,4′-dicarboxylic acid-2,2′-bipyridine and two bipyridines each of which had electron donating dialkylamine substituents in the 4 and 4′ positions. The electronic absorption spectra exhibited absorptions that moved to lower energy as the donor ability of the amine substituent increased. Density functional calculations established that the HOMO was delocalized over the metal and two pyridine groups located *trans* to the pyridines of the dicarboxylic acid bipyridine. The LUMO was delocalized over the dicarboxylic acid bipyridine. Cyclic voltammetry of the deprotonated compounds exhibit one quasi-reversible oxidation and three reductions. Coupled with the emission data, the excited state reduction potentials were estimated to range from −0.93 to −1.03 V *vs.* NHE. Monodispersed 3.2 nm diameter nanocrystals (NCs) of zinc oxide were found to quench partially the excited state of the dyes *via* a static quenching electron transfer process involving the formation of a dyad of the complex and the NC. The magnitude of the partial quenching of complexed dyes was correlated to the distribution of band gaps for the NCs, which is an inverse function of diameter. Dyes attached to the NCs on the small end of the particle size distribution had electron transfer rates that were uncompetitive with radiative and nonradiative decay mechanisms.

Introduction

Interfacial electron transfer from the photoexcited state of a sensitizer to the conduction band of the metal oxide semiconductor is an important event leading to charge separation in dye-sensitized solar cells.[1–4] The dynamics of this process have been examined with a variety of time-resolved and steady-state spectroscopic methods on metal oxide nanocrystal films.[4–7] The heterogeneous nature of the surface environment, however, complicated electron transfer dynamics leading to multiple injection time scales for a given sensitizer.[5,8–14] Substitution of the nanocrystalline film with monodispersed metal oxide nanocrystals (NCs) offers an alternative with a potentially more uniform environment. This has recently been done using TiO_2 dispersions, where injection times were too fast to be measured accurately.[6,15] Zinc oxide (ZnO) offers similar properties to TiO_2, but has the added advantage that synthetic routes are available that generate monodispersed NCs that are stable in common solvents and are optically transparent.[16]

In previous work we demonstrated that ZnO NCs quenched the excited state by electron transfer of two carboxylate-bound fluorophores, a terthiophene derivative and a zinc porphyrin.[17–19] Although capable of binding to the ZnO NCs, the ruthenium-polypyridyl complex, $[Ru(bpy)_2(dcbpy)](PF_6)_2$ where bpy = 2,2′-bipyridine and dcbpy = 4,4′-dicarboxylic acid-2,2′-bipyridine, exhibited fluorescence that was not quenched. This was initially unexpected based on the reported fluorescence quenching of $[Ru(bpy)_2(dcbpy)]^{2+}$ when it was bound to a colloidal ZnO film.[20] Hypothesizing that its excited state was not sufficiently reducing, in this report we describe the preparation of a series of ruthenium complexes in which two amine-substituted bipyridines serve to increase the excited state reduction potential of the complex.[21–24] The third bipyridine, dcbpy, is also present as a means to attach the dye to the ZnO NCs. The amines increased the excited state potential by approximately 0.2 V and partial fluorescence quenching by the NCs was observed. Proton NMR spectroscopy served as an independent assessment of binding the dye to the NCs.

Results

Ruthenium complexes

Fig. 1 shows the structure of the six ruthenium complexes each of which comprise two different bipyridine ligands.

Department of Chemistry, University of Minnesota, 207 Pleasant St. SE, Minneapolis, MN 55455, USA. E-mail: wlg@umn.edu

†Electronic supplementary information (ESI) available. See DOI: 10.1039/c4dt03272a

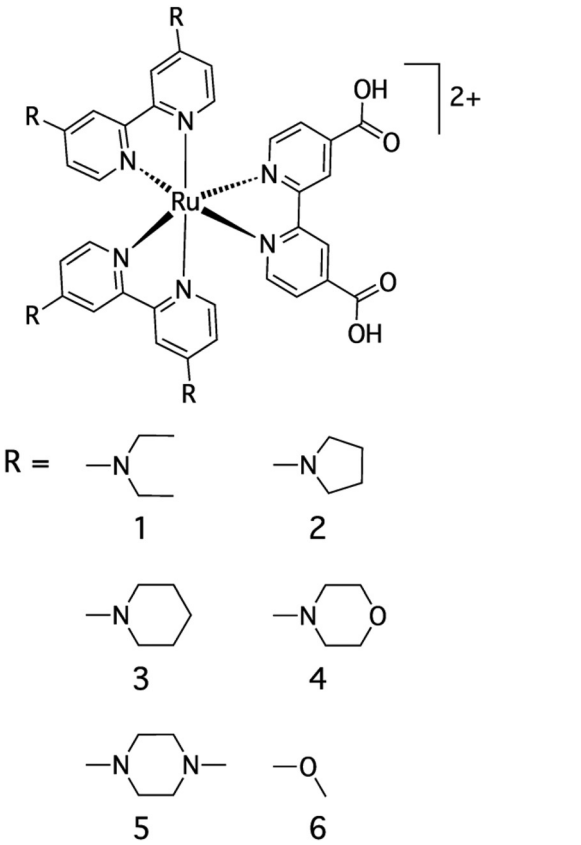

Fig. 1 Molecular structure of the substituted tris-bipyridine ruthenium complexes (**1–6**).

Common to all is the 4,4′-dicarboxylic acid-2,2′-bipyridine (dcbpy), which binds the complexes to the ZnO NCs through the carboxylate groups. The remaining two bipyridines were substituted in the 4 and 4′ positions with strong electron donating dialkylamino substituents. All syntheses were based on known methods. Compounds **1–4** were prepared by reaction of dcbpy and triethylamine with the paramagnetic bis-(bipyridine) intermediates, $[Ru(R_2bpy)_2Cl_2]Cl$. The latter complexes were prepared using the method of Viala and Coudret,[25] which was expected to yield the divalent ruthenium compounds, $Ru(R_2bpy)_2Cl_2$. Presumably the dialkylamino substituents help to stabilize the trivalent ruthenium compounds, which were the observed products. With the methoxy substituent, the corresponding Ru^{2+} compound was formed as expected and subsequently reacted with dcbpy to yield **6**. With the *N*-methylpiperazino substituent, the initial reaction proceeded directly to $\{Ru[(mepipz)_2bpy]_3\}Cl_2$, thus precluding its use for the synthesis of **5**. The successful alternative synthesis of **5** involved reaction of $\{[(\eta^6\text{-}p\text{-cymene})RuCl]_2(\mu\text{-}Cl)_2\}$ with two equivalents of dcbpy in DMF followed by addition of a slight excess of $(mepipz)_2bpy$ and reflux.

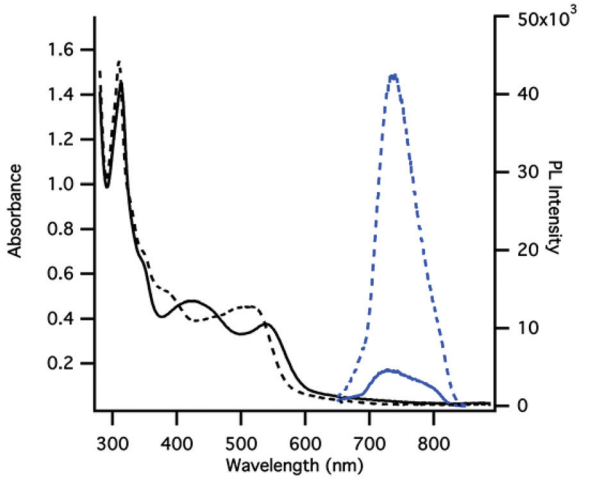

Fig. 2 Absorption (black) and emission (blue) of **1** (solid lines) and **1-CO$_2^-$** (dashed lines) with $[Me_4N][OH]$ in methanol. When one equivalent of additional H^+ is added, the emission of **1** disappears.

The compounds were characterized using mass spectrometry and electronic absorption, luminescence, infrared and ^1H NMR spectroscopies, and cyclic voltammetry. Compound **1** was also characterized by elemental analysis. Table 1 lists the longest wavelength absorption and emission maximum for each of the deprotonated dyes. A complete tabular listing of the electronic absorption maxima and extinction coefficients for both the protonated and deprotonated dyes is available in the ESI Table 1.† Fig. 2 displays the absorption spectra of **1** and **1-CO$_2^-$**. The complexes have intense absorptions around 315 nm corresponding to the bipyridine π–π^* transitions. In the visible region, all complexes have absorptions from 400–600 nm with molar extinction coefficients ranging from 12 000–20 000 M^{-1} cm^{-1} attributed to metal to ligand charge transfer transitions. The lowest energy absorptions in compounds **1–6** exhibit an approximate corre-

Table 1 Spectroscopic and electrochemical properties of deprotonated **1–6**

Dye anions	λ_{abs}[a] (nm)	λ_{em}[a,b] (nm)	E^{o}[c] (V) Ru^{III}/Ru^{II}	E^{o}[c] (V) RuL_3^{2+}/RuL_3^{+}	E^{o}[c] (V) RuL_3^{+}/RuL_3^{0}	E^{o}[c] (V) RuL_3^{0}/RuL_3^{-}	$E^{\star}$[d] Ru^{III}/Ru^{II}
1-COO$^-$	515	748	0.832	−1.40	−1.71	−1.92	−0.99
2-COO$^-$	520	752	0.779	—	—	—	−1.03
3-COO$^-$	502	742	0.865	−1.37	−1.64	−1.82	−0.96
4-COO$^-$	499	723	0.942	−1.33	−1.55	−1.76	−0.94
5-COO$^-$	498	725	0.940	−1.34	−1.58	−1.78	−0.93
6-COO$^-$	475	680	1.22	−1.20	−1.36	−1.57	−0.76

[a] Measured in CH_3OH at 25 °C. [b] $\lambda_{Excit} = \lambda_{abs}$. [c] Recorded under argon at 100 mV s^{-1} using $[^nBu_4N][PF_6]$ as the supporting electrolyte in dimethylformamide and referenced to a Ag/AgCl electrode. All potentials are listed *vs.* NHE. [d] Excited state reduction potential.

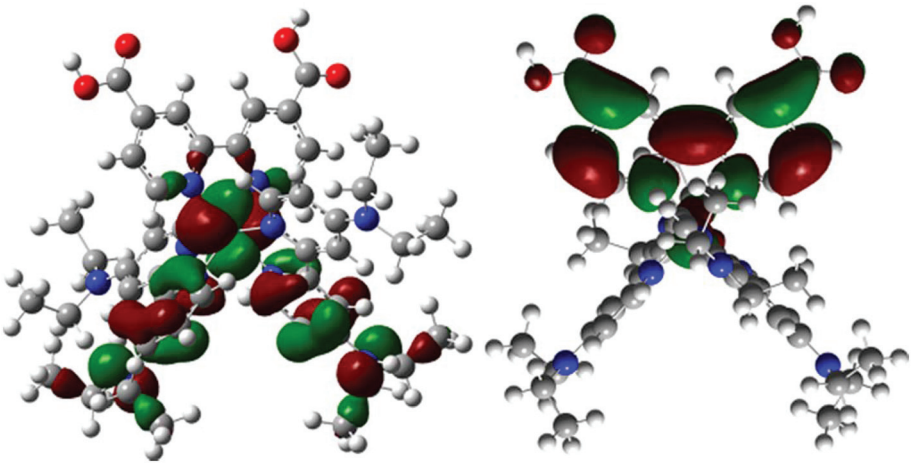

Fig. 3 HOMO (left) and LUMO (right) of **1**.

lation with the donor characteristics of the bipyridine substituents. For **1-CO$_2^-$**, λ_{max} appears at 515 nm, while for **6-CO$_2^-$** it shifts to 475 nm.

The push–pull nature of the electronic structures of **1–6** is evident from density functional calculations. Fig. 3 shows DFT (B3LYP) results that verify the LUMO resides primarily on the dcbpy ligand and that the HOMO resides on the ruthenium metal center and extends onto the amino-substituted bipyridine rings and the amino nitrogen. The ligand-based orbitals contributing to the HOMO involve one-half of each of the amino-substituted bipyridine ligands, each of which is oriented in the *xy*-plane (defined as the plane of the dcbpy ligand) for favorable π-overlap with the Ru d_{xy} orbital. The antibonding nature of this interaction emphasizes the strong π-donor property of the amino-bpy groups, thus raising the energy of this orbital. The next highest occupied molecular orbitals exhibit a similar interaction between the pyridine groups (perpendicular to the Ru-dcbpy plane) and the Ru d_{xz} and d_{yz} orbitals. The results for the remaining complexes, including {Ru[(Et$_2$N)$_2$bpy]$_2$[(Cl)$_2$bpy]}(PF$_6$)$_2$ are similar to the results obtained for **1** presented in Fig. 3. As noted by others,[26] when push–pull chromophores used in dye-sensitized solar cells are attached to the semiconductor *via* the functional group (carboxylates is many cases) on the "pull" end, the electron in the excited state is conveniently localized near the point of attachment. This is expected to increase the efficiency of electron transfer.

Deprotonation of **1–6** using [Me$_4$N][OH] causes a blue-shift in the MLCT bands. The deprotonated form of each compound exhibits a weak emission with a λ_{max} listed in Table 1. For **1-CO$_2^-$**, the emission is also plotted in Fig. 2. The very weak emission observed from solutions of pure **1** disappears following addition of acid suggesting that it may be due to residual **1-CO$_2^-$**.[27] The infrared spectra in KBr (ESI Fig. 2†) of the amino-substituted compounds **1**, **3** and **4** exhibit distinct absorptions at 1700 cm^{-1} attributable to the carboxylic acid. For **2** and **5**, the lack of a specific absorption at 1700 cm^{-1} is likely due to strong H-bonding, or even the possible existence

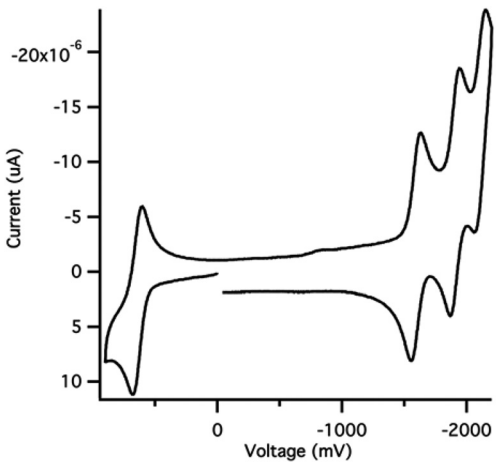

Fig. 4 Cyclic voltammagrams of **1-CO$_2^-$** in DMF with 0.1 M [^{n}Bu$_4$N][PF$_6$] as the supporting electrolyte. The sample was degassed with argon and referenced to a Ag/AgCl electrode.

of a zwitterionic structure, in the solid state. Deprotonation of **1** leads to disappearance of the 1700 cm^{-1} absorbance, but the C–O stretch of the carboxylate is obscured by the intense aromatic C–C vibrations.

Cyclic voltammetry, shown in Fig. 4 for **1-CO$_2^-$** and listed in Table 1 for the deprotonated dyes, was used to analyze the redox processes in the complexes. Compounds **1–6** show reversible Ru^{III}/Ru^{II} oxidations between 0.80 and 1.37 V *versus* NHE and irreversible reductions between −0.84 and −1.92 V. Because it is the deprotonated state of the dyes that bind to the NCs, we have focused our attention primarily on these. Compounds **1-CO$_2^-$** to **6-CO$_2^-$** become easier to oxidize as the Ru^{III}/Ru^{II} couple is shifted to lower potentials (0.78–1.22 V). Also, upon deprotonation, three reversible reductions are now evident for the three bipyridine ligands of each of the compounds. The difference between the first and second bpy reduction potential is slightly larger then that potential difference between the second and third reduction. This is consist-

ent with assigning the least negative reduction to the dcbpy ligand.[28] Also consistent with this assignment, the second and third reduction potentials are more sensitive to changing the dialkylamino substituents. Typically, for heteroleptic Ru(II) coordination compounds the first ligand reduced electrochemically is also the same ligand on which the excited state is localized in the thermally equilibrated excited state.[29] Based on the cyclic voltammetry, the relaxed MLCT excited state is attributed to $[Ru^{III}(aminobpy)_2(dcbpy^-)]^{2+}$*, where the negative charge is localized upon the ligand that binds to ZnO.

In the absence of direct measurement of the energy difference between the singlet and triplet excited states of the complexes, the excited reduction potentials were estimated using the method reported by Thomson and coworkers.[30] This involves adding the energy of the λ_{max} value for room temperature emission to the standard reduction potential for the Ru^{3+} complex and subtracting from this result a correction constant of 0.17 V, which was derived from more detailed studies of six tris-(substituted-bipyridine) ruthenium complexes. In addition a smaller correction of 0.03 V was added due to the entropy change at 300 K associated with the change in spin multiplicity. Values for E^* range from −1.03 to −0.76 V for **2** to **6**, respectively (Table 1). Considering that the size-dependent conduction band minimum (CBM) of 3.2 nm ZnO NCs is approximately −0.5 V *vs.* NHE, the ΔG° for quenching the excited state will be negative for all of the dyes.

Probing complex binding to ZnO NCs

NMR spectroscopy was used to quantify the extent of dye attachment to the surface of the NCs. Upon binding, the dye resonances broaden and disappear into the baseline. This can be attributed to the slow rotation of the dyad, hindered motion of the molecule on the surface[31] and, possibly, to heterogeneity in the binding sites on the surface of the NC.[32–34] Fig. 5 shows the aromatic region of the ^{1}H NMR spectra of pure **1** and **1-CO$_2^-$**, as well as in the presence of increasing amounts of ZnO NCs. The concentration of **1** is held constant as the concentration of ZnO NCs is increased in successive samples. With increasing NC concentration the resonances of the protonated form decrease in intensity and shift upfield to peaks characteristic of **1-CO$_2^-$**. The three resonances furthest downfield represent the aromatic hydrogens of the dcbpy ligand, with the resonance at 9 ppm attributed to the 3 and 3′ hydrogens *ortho* to the acid group. These hydrogens are expected to be the most sensitive to the protonation state of the complex. Resonances associated with the $[(Et_2N)_2bpy]$ ligands are not affected significantly. At ratios of 20 : 1 and 10 : 1 signals due to free **1-CO$_2^-$** are still detectable, however, at 2 : 1 all resonances are indistinguishable from the baseline indicating all dyes are bound. Based on estimates of the van der Waal radii of the complexes, we suggest that a maximum of six dyes could bind to a 3.2 nm NC. Conducting this set of experiments using **6** produced similar results, although disappearance of the dye resonances occurred at a lower dye to NC ratio.

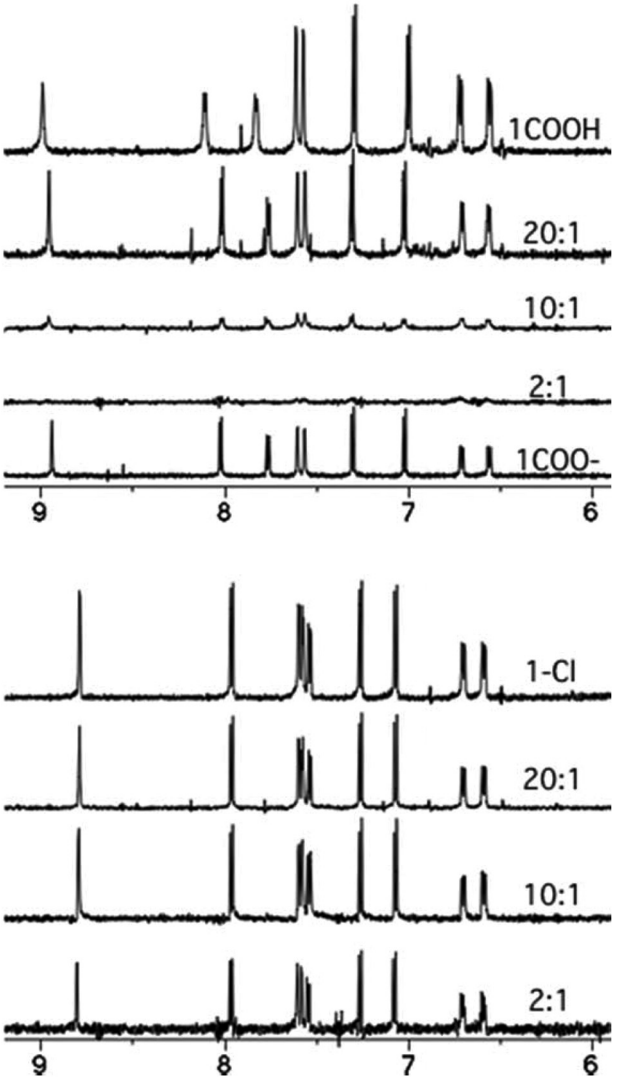

Fig. 5 ^{1}H NMR spectra of the aromatic region of **1** : ZnO (top) and **1-Cl** : ZnO (bottom) dyads at the given ratios.

To verify that the broadening and eventual disappearance of the aromatic signals of **1-CO$_2^-$** and **6-CO$_2^-$** was the result of attachment to the surface of the NCs, the same set of measurements were made using $\{Ru[(Et_2N)_2bpy]_2[(Cl)_2bpy]\}(PF_6)_2$ where the carboxylic acid groups were replaced with chloro substituents. As with **1-CO$_2^-$**, the concentration of the ruthenium complex was held constant while the concentration of the ZnO was increased with each successive sample. The spectra in Fig. 5 of 20 : 1 through 2 : 1, exhibited no change in the intensity or width of the peaks as the NCs were added. This indicates that the acid functionality is necessary for binding to the surface of the NCs.

Excited state quenching using ZnO NCs

Steady state Stern-Volmer quenching analysis was performed on the dyads described above using a constant concentration of dye and an increasing amount of ZnO nanocrystals and comparing the emission to that of the deprotonated dye. Fig. 6

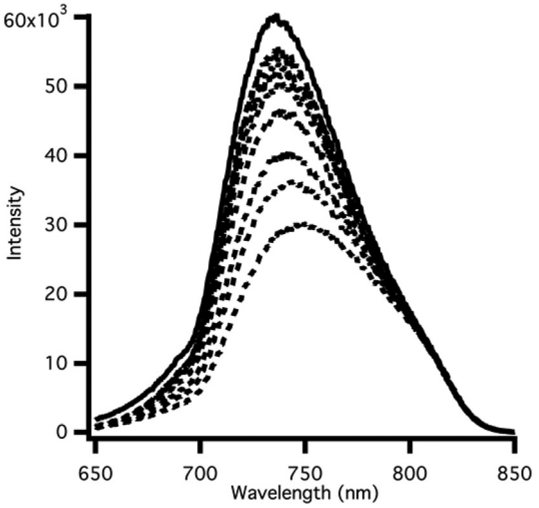

Fig. 6 Emission from methanol solutions of pure **1-CO_2^-** (solid line), (**1-CO_2^-**)$_n$ZnO dispersions with subsequent additions of ZnO NCs at constant dye concentration. As the concentration of ZnO increases the emission intensity decreases to the final sample of 2 : 1 (λ_{ex} = 415 nm).

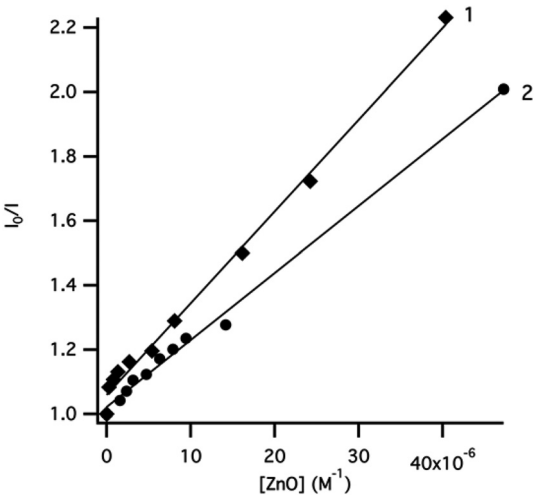

Fig. 7 Stern-Volmer plot of **1** (diamonds) and **2** (circles).

shows the emission of **1-CO_2^-** at various ZnO ratios from 120 : 1 to 2 : 1. As the NC concentration increases, the emission intensity decreases by a factor of 0.51 of the **1-CO_2^-** alone. From the slope of the Stern-Volmer plot, Fig. 7, the association constant (K_{sv}) was calculated to be 2.4 × 10^4 M^{-1}. While the complexes exhibit different amounts of quenching, the relationship of I_0/I *versus* concentration was linear in all cases. Table 2 lists the Stern-Volmer association constants for the amino-substituted bipyridine complexes and Fig. 7 shows the Stern-Volmer plot for complexes **1-CO_2^-** and **2-CO_2^-**.

As the value of K_{sv} decreases, the fraction of excited states that are quenched also decreases in a pattern that correlates roughly with excited state potential. The complexes with amine substituents (**1–5**) have excited state potentials clustered around −1 V. Complex **6** has the lowest excited state value, at

Table 2 Stern-Volmer association constants for the corresponding dye on 3.2 nm ZnO nanocrystals in methanol

Dye	**1**	**2**	**3**	**4**	**5**
K_{SV} (M^{-1} × 10^{-4})	3.1	2.6	2.2	1.7	1.5
Fraction quenched at 2 : 1 dye : NC	0.51	0.50	0.54	0.43	0.39

−0.76 V, and does not show any quenching. Because we know **6** attaches to the surface of the ZnO NCs, the excited state must not be of sufficient energy for electron transfer to be competitive with competing radiative and nonradiative decay mechanisms.

While these Stern-Volmer experiments prove that ZnO is capable of quenching the emission of the excited dye, they do not establish the mechanism. We assign the mechanism to electron transfer based on three factors. First, in previous reports of dyads comprising ZnO NC with terthiophene or porphyrin chromophores bound *via* carboxylates, ultrafast spectroscopic methods provided direct evidence for the formation of an oxidized dye thus confirming the electron transfer quenching mechanism.[17,18] Second, given the large energy differences between the emission wavelengths of the dyes in this study and the ZnO NC absorption, resonant energy transfer can be ruled out as a quenching mechanism. Finally, there was no evidence that concentration quenching is significant, as has been found in related systems.[35] It is possible that electron injection could occur into surface trap states that exist on metal oxide nanoparticles instead of into the empty conduction band. In studies of excited state charge injection from N3 into ZrO_2, surface trap states were shown to serve as the electron acceptor.[36]

Discussion

While we are ultimately interested in measurement of the rates of electron transfer to ZnO NCs from a series of structurally similar donors, we discuss here a noteworthy correlation between the fraction of static quenching and the excited state energy of the dyes. Proton NMR spectroscopy established that at a 2 : 1 molar dye to NC ratio all dyes present in the mixture were bound to the ZnO NCs. Further, by comparison of spectroscopic changes in **1–6** *vs.* the lack of any observed changes for {Ru[$(Et_2N)_2$bpy]$_2$[$(Cl)_2$bpy]}$(PF_6)_2$ the NMR data confirm that the carboxylates present in **1–6** are integral to dye binding and that the process involves static quenching.

Despite NMR evidence that all dyes were bound to NCs, at the 2 : 1 dye to NC ratio at most half of the excited states were quenched. The fraction of quenching correlated with the excited state potential. No quenching was observed for the methoxy-substituted bpy derivative **6**, which had the least negative E^* (−0.76 V). For the dialkylamino-substituted compounds, the fraction quenched ranged from 0.39 for **5** (E^* = −0.93 V) to 0.54 for **2** (E^* = −1.03 V). Two possible explanations could explain the lowered quenching yields of bound dyes.

First, based on studies of nanocrystalline ZnO films[37] adsorption of dye molecules can lead to precipitates that are not electronically coupled to the core of the ZnO NCs, thus reducing the electron transfer yield. While the nature of the precipitates has not been defined, as long as they lead to line broadening in the NMR spectrum without quenching emission from the dye, this could contribute to the low quenching yield.

An alternative explanation that is not mutually exclusive with the possible formation of precipitates is that the trend in quenching yield correlates to the distribution of diameters associated with the ZnO NC synthesis. The ZnO NCs used in this study had a mean diameter of 3.2 nm. Assuming a Gaussian distribution of NC diameters with a standard deviation of 0.32 nm (±10%),[16] we expect an associated distribution of energies for the conduction band minima (CBM). This means that a fraction of the dyes will be bound to smaller NCs where the corresponding decreased rate of electron transfer becomes uncompetitive with the rates of emission and/or nonradiative decay. Although we use the term conduction band minimum, we recognize that as the NCs decrease in diameter the density of states decreases and the energy of the lowest empty state rises. In quantum confined NCs, the lowest empty state is the S_e state.[38]

Fig. 8 attempts to summarize the factors contributing to this explanation. For each of the dyes the experimental fraction of *unquenched* dye is plotted on the *x*-axis as a function of *E** on the *y*-axis. The solid line shows the energy of the CBM as a function of the NC diameter (top axis). This was calculated using the values for the change in the band gap as a function of size reported by Sarma and coworkers[39] and adding it to the bulk ZnO band gap and the work function measured on a nanocrystalline ZnO film.[40] This calculation assigns the entire size-dependent change in the band gap to a change in the CBM; an assumption that over estimates its impact. This relationship allowed the conversion of the Gaussian NC size distribution to a NC CBM distribution, which is plotted as a dashed line. Integration of the distribution (dotted line) shows the fraction of the NCs on the *x*-axis that have a conduction band minimum above the energy shown on the *y*-axis. The curve is offset from the experimental data by 0.44 V. Although the overestimate of the CBM will contribute a small amount to this offset, we suggest that the reorganization energy (λ) associated with the electron transfer is the major factor. Reorganization energies for electron transfer to and from nanocrystalline metal oxide films or colloidal dispersions range from 0.3–2 V.[1]

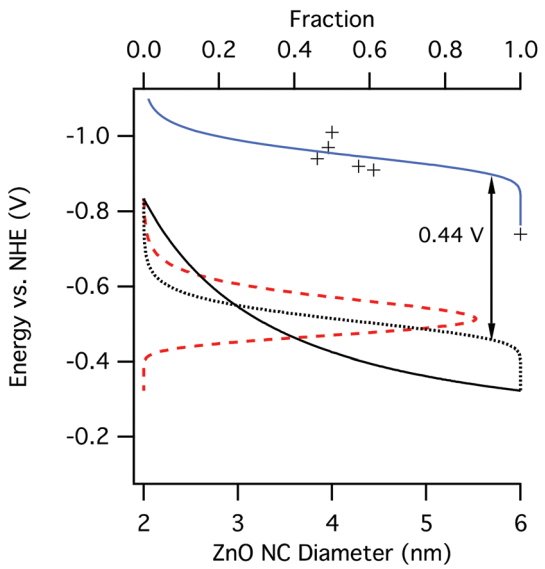

Fig. 8 The solid black line shows the ZnO NC conduction band minimum (CBM) energy as a function of NC diameter. The dashed red line shows the CBM energy distribution for a 10% Gaussian distribution in NC diameter centered at 3.2 nm. Integration of this distribution (dotted line) shows the fraction of particles (top axis) having a CBM energy above the value shown on the vertical axis. The + symbols show the experimental fraction of unquenched dye as a function of *E**. The solid blue line shows the integrated distribution (dotted line) raised in energy by 0.44 V.

Conclusions

A series of electron-rich, heteroleptic tris-bipyridine ruthenium complexes were synthesized and characterized. Two of the bpy ligands were substituted with electron releasing dialkylamino substituents in the 4 and 4′ positions while the third ligand was dcbpy, which allowed the complex to be anchored to the surface of ZnO NCs. The dialkylamino groups raised the excited state reduction potential of the complex by at least 0.2 V compared to $[Ru(bpy)_2(dcbpy)]^{2+}$. This increase was sufficient to allow a significant fraction of the excited states to be quenched by charge injection into the ZnO NCs having a mean diameter of 3.2 nm. The fraction of quenched dyes was correlated to the NC size distribution as a result of the impact of quantum confinement on the energy of the conduction band minimum. The excited states of dyes bound to NCs on the smaller end of the distribution continued to decay by fluorescence and nonradiative pathways. This observation may be important in constructing ZnO-based dye-sensitized solar cells from NC dispersions. While smaller ZnO particles can have the beneficial effect of increasing the effective surface area per mole of ZnO and therefore the dye loading, particles that are too small would reduce the yield of charge separation and potentially the overall cell efficiency. Further work is in progress to measure the effect of ZnO NC diameter on the charge injection yield and the rate of charge injection using ultrafast spectroscopic methods.

Experimental

Materials

Ruthenium(III) chloride trihydrate ($RuCl_3 \cdot 3H_2O$) was purchased from Pressure Chemical Company and used as received. Spectroscopic grade methanol, 2,2′-bipyridine, 4,4′-dimethyl-2,2′-bipyridine, diethylamine, pyrrolidine, piperidine, morpho-

line, *N*-methylpiperazine, tetramethylammonium hydroxide ($NMe_4OH{\cdot}5H_2O$), and zinc acetate ($Zn\text{-}(CH_3COO)_2{\cdot}2H_2O$), were purchased from Sigma Aldrich and used as received. All additional solvents were dried (unless water was used as a co-solvent) and deoxygenated before use, and all procedures were performed using standard Schlenk techniques. 4,4′-Dicarboxylic acid-2,2′-bipyridine (dcbpy), 4,4′-dichloro-2,2′-bipyridine-*N*,*N*′-dioxide, 4,4′-dichloro-2,2′-bipyridine [$(Cl)_2$bpy], 4,4′-bis(diethylamino)-2,2′-bipyridine [$(Et_2N)_2$bpy], 4,4′-dipyrrolidino-2,2′-bipyridine [$(pyrrol)_2$bpy], 4,4′-dipiperidino-2,2′-bipyridine [$(pip)_2$bpy], 4,4′-dimorpholino-2,2′-bipyridine [$(morph)_2$bpy], 4,4′-di(*N*-methylpiperazino)-2,2′-bipyridine, [$(mepipz)_2$bpy] 4,4′-dimethoxy-2,2′-bipyridine [$(MeO)_2$bpy], were prepared according to literature procedures.[41–43] Synthetic details and ^{1}H NMR spectroscopic data for the methoxy- and amino-substituted bipyridines are available in the ESI.† Preparation of the intermediate bis-substituted bipyridine ruthenium complexes was based on the report by Viala and Coudret,[25] however, for the amino-substituted bipyridine ligands the reducing agents (glucose and ascorbic acid) were not strong enough to form the divalent ruthenium dichloro complexes. Following chromatographic purification the formation of the paramagnetic Ru^{3+} complex ions was confirmed by mass spectrometry, and the powders were used in subsequent preparation of the target dye molecules. Details are available in the ESI.†

Methods

Unless otherwise noted, all NMR spectra of the complexes and ligands were taken on a Varian Inova 300 MHz spectrometer and chemical shifts were referenced to the residual solvent peak. All NMR spectra of dye:ZnO dyads were taken on a Varian Inova 500 MHz spectrometer and chemical shifts were referenced to the residual solvent peak. Mass spectral data were taken on a Bruker BioTOF II in ESI-TOF mode. Electronic absorption spectra were collected on an Ocean Optics DH-2000-BAL spectrometer. The steady-state emission spectra were recorded on a Spex Fluorolog 1680 0.22 m double spectrometer equipped with a xenon source. Front face fluorescence spectra were corrected to compensate for changes in the instrument's sensitivity at longer wavelengths. UV-visible and fluorescence spectroscopic measurements were performed in quartz cuvettes with a 3 mm path length unless otherwise noted. The IR spectra of ruthenium complexes (KBr pellet) were recorded on a Nicolet MAGNA-IR 560 spectrometer.

Electrochemistry

Cyclic voltammograms were obtained on a BAS-100B electrochemical analyzer using methods previously described.[44] All solutions were prepared in acetonitrile or dimethylformamide with 0.1 M tetrabutylammonium hexafluorophosphate [TBA][PF_6] as the supporting electrolyte and degassed with argon. Reported $E°$ potentials were referenced to a Ag/AgCl electrode and are reported *versus* NHE. The $E°$ ferrocenium/ferrocene couple was measured under identical conditions and used to correct the reported potentials. In 0.1 M [TBA][PF_6]/DMF its $E°$ was 0.515 V (literature 0.495 V *versus* Ag/AgCl).[45]

Density functional calculations

Compounds **1**, **3** and **5** were fully optimized at the density functional level of theory using the B3LYP functional and the 6-31G* basis set for all elements except ruthenium. The 6-31G** basis set was used for **2**, **4** and {Ru[$(Et_2N)_2$-bpy]$_2$[$(Cl)_2$bpy]}$(PF_6)_2$. For all compounds the SDD basis set was used for ruthenium. All calculations were performed using the Gaussian 09 software suite.[46]

Synthesis of {Ru[$(Et_2N)_2$bpy]$_2$dcbpy}$(PF_6)_2$, 1.[47] A mixture of {Ru[$(Et_2N)_2$bpy]$_2Cl_2$}Cl (0.30 g, 0.38 mmol, 1 eq.), dcbpy (0.27 g, 1.1 mmol, 3 eq.) and triethylamine (0.90 mL, 6.4 mmol, 17 eq.) was added to 25 mL of ethanol–water (4 : 1) and heated at reflux for 3 h. The solvent was evaporated and the resulting complex was chromatographed on a Sephadex LH-20 column using acetonitrile–isopropanol (90 : 10) as eluent. The first band to elute yielded a red solid following removal of the solvent. This was dissolved in a minimum of water and the desired complex was precipitated with the addition of excess $NaPF_6$ and isolated by filtration to give 0.37 g (80%) of **1**. ^{1}H-NMR (300 MHz; CD_3CN): δ 9.48 (s br, 2H), 8.07 (d, J = 5.9 Hz, 2H), 7.82 (dd, J = 5.9, 1.3 Hz, 2H), 7.40 (d, J = 2.7 Hz, 2H), 7.36 (d, J = 2.7 Hz, 2H), 7.19 (d, J = 6.8 Hz, 2H), 6.90 (d, J = 6.8 Hz, 2H), 6.61 (dd, J = 6.8, 2.7 Hz, 2H), 6.40 (dd, J = 6.9, 2.7 Hz, 2H), 3.54 (q, J = 7.0 Hz, 8H), 3.47 (q, J = 7.1 Hz, 8H), 1.19 (t, J = 7.0 Hz, 12H), 1.13 (t, J = 7.0 Hz, 12H). HR ESI-MS m/z (obs) 471.1930 (M^{2+}), m/z (calcd): 471.1921. Elem. Anal. Obs. C, 46.41; H, 4.78; N, 11.25. Calcd C 46.79; H, 4.91; N, 11.37.

Synthesis of {Ru[$(pyrrol)_2$bpy]$_2$dcbpy}$(PF_6)_2$, 2. Using the same procedure as above, {Ru[$(pyrrol)_2$bpy]$_2Cl_2$}Cl (0.15 g, 0.18 mmol) was reacted with dcbpy (0.14 g, 0.56 mmol, 3 eq.), and triethylamine (0.50 mL, 3.2 mmol, 17 eq.). Compound **2** was the first band to elute from a Sephadex LH-20 column using acetonitrile–methanol (90 : 10) as eluent. The isolated yield was 0.17 g (75%). ^{1}H-NMR (300 MHz; CD_3OD): δ 8.95 (s br, 2H), 8.00 (d, J = 5.8 Hz, 2H), 7.73 (dd, J = 5.8, 1.5 Hz, 2H), 7.55 (d, J = 2.5 Hz, 2H), 7.51 (d, J = 2.5 Hz, 2H), 7.27 (d, J = 6.6 Hz, 2H), 7.01 (d, J = 6.6 Hz, 2H), 6.53 (dd, J = 6.7, 2.5 Hz, 2H), 6.42 (dd, J = 6.7, 2.5 Hz, 2H), 3.56–3.37 (m, 16H), 2.16–2.00 (m, 16H). HR ESI-MS m/z (obs) 467.1614 (M^{2+}), m/z (calcd) 467.1608.

Synthesis of {Ru[$(pip)_2$bpy]$_2$dcbpy}$(PF_6)_2$, 3. Using the same procedure as above, {Ru[$(pip)_2$bpy]$_2Cl_2$}Cl (0.13 g, 0.15 mmol) was reacted with dcbpy (0.11 g, 0.46 mmol, 3 eq.), and triethylamine (0.37 mL, 2.6 mmol, 17 eq.). Compound **3** was the first band to elute from a Sephadex LH-20 column using acetonitrile–isopropanol (90 : 10) as eluent to yield 0.13 g (68% yield). ^{1}H-NMR (300 MHz; CD_3CN): δ 9.10 (s br, 2H), 8.14 (d, J = 5.9 Hz, 2H), 7.82 (d, J = 5.9 Hz, 2H), 7.67 (d, J = 2.5 Hz, 2H), 7.63 (d, J = 2.3 Hz, 2H), 7.21 (d, J = 6.8 Hz, 2H), 6.93 (d, J = 6.8 Hz, 2H), 6.76 (dd, J = 6.8, 2.6 Hz, 2H), 6.56 (dd, J = 6.7, 2.3 Hz, 2H), 3.69–3.42 (m, 16H), 1.80–1.51 (m, 24H). HR ESI-MS m/z (obs) 495.1940 (M^{2+}), m/z (calcd) 495.1921.

Synthesis of {Ru[(morph)$_2$bpy]$_2$dcbpy}(PF$_6$)$_2$, 4. Using the crude mixture of {Ru[(morph)$_2$bpy]$_2$Cl$_2$}Cl and an excess of dcbpy, the reaction was completed as above and **4** was purified on a Sephadex LH-20 column using acetonitrile–methanol (90 : 10) as eluent to yield 0.18 g (20% yield based on the amount of $RuCl_3{\cdot}3H_2O$ used for the preparation {Ru[(morph)$_2$bpy]$_2$Cl$_2$}Cl). ^{1}H-NMR (300 MHz; CD_3CN): δ 9.64 (s br, 2H), 7.99 (d, J = 5.8 Hz, 2H), 7.80 (d, J = 6.0 Hz, 2H), 7.68 (d, J = 2.2 Hz, 2H), 7.65 (d, J = 2.4 Hz, 2H), 7.28 (d, J = 6.7 Hz, 2H), 7.06 (d, J = 6.7 Hz, 2H), 6.75 (dd, J = 6.7, 2.3 Hz, 2H), 6.58 (dd, J = 6.7, 2.6 Hz, 2H), 3.79 (t, J = 4.7 Hz, 8H), 3.74 (t, J = 4.7 Hz, 8H), 3.50 (t, J = 4.7 Hz, 8H), 3.43 (t, J = 4.4 Hz, 8H). HR ESI-MS m/z (obs) 499.1517 (M^{2+}), m/z (calcd) 499.1506.

Synthesis of {Ru[(MeO)$_2$bpy]$_2$dcbpy}(PF$_6$)$_2$, 6. Using the same procedure as above, the crude mixture containing Ru[(MeO)$_2$bpy]$_2$Cl$_2$ (0.47 g, 0.74 mmol) was reacted with dcbpy (0.55 g, 2.2 mmol, 3 eq.), and triethylamine (1.50 mL, 11.1 mmol, 15 eq.). Due to solubility, **6** was first converted to the PF_6^- salt with $NaPF_6$ and purified on a Sephadex LH-20 column using acetonitrile–methanol (90 : 10) as eluent to yield 0.62 g (80% yield). ^{1}H-NMR (300 MHz; CD_3CN): δ 9.02 (d, J = 1.2 Hz, 2H), 8.03–8.00 (m, 6H), 7.80 (dd, J = 5.9, 1.7 Hz, 2H), 7.50 (d, J = 6.5 Hz, 2H), 7.36 (d, J = 6.5 Hz, 2H), 7.00 (dd, J = 6.5, 2.7 Hz, 2H), 6.89 (dd, J = 6.6, 2.7 Hz, 2H), 4.01 (s, 6H), 3.97 (s, 6H). HR ESI-MS m/z (obs) 389.0683 (M^{2+}), m/z (calcd) 389.0662.

Synthesis of {Ru[(Et$_2$N)$_2$bpy]$_2$[(Cl)$_2$bpy]}(PF$_6$)$_2$. Using the same procedure as above, {Ru[(Et$_2$N)$_2$bpy]$_2$Cl$_2$}Cl (0.21 g, 0.26 mmol) was reacted with (Cl)$_2$bpy (0.18 g, 0.78 mmol, 3 eq.), and triethylamine (0.73 mL, 5.2 mmol, 17 eq.). The product was purified on a Sephadex LH-20 column using acetonitrile–isopropanol (90 : 10) as eluent to yield 0.16 g (52% yield). ^{1}H-NMR (500 MHz; CD_2Cl_2): δ 8.24 (d, J = 2.1 Hz, 2H), 7.88 (d, J = 6.1 Hz, 2H), 7.41 (dd, J = 6.2, 2.2 Hz, 2H), 7.23–7.19 (m, 6H), 6.96 (d, J = 6.8 Hz, 2H), 6.56 (dd, J = 6.8, 2.9 Hz, 2H), 6.44 (dd, J = 6.8, 2.8 Hz, 2H), 3.50 (q, J = 7.1 Hz, 8H), 3.45 (q, J = 7.1 Hz, 8H), 1.25 (t, J = 7.1 Hz, 12H), 1.21 (t, J = 7.1 Hz, 12H). HR ESI-MS m/z (obs) 461.1641 (M^{2+}), m/z (calcd) 461.1633.

Synthesis of {Ru[(mepipz)$_2$bpy]$_2$dcbpy}(PF$_6$)$_2$, 5. The glucose reaction was unsuccessful at producing {Ru[(mepipz)$_2$bpy]$_2$Cl$_2$}Cl as all ruthenium went directly to the tris-(mepipz)$_2$bpy ruthenium complex when (mepipz)$_2$bpy was added. This was confirmed through NMR and ESI-MS as only the {Ru[(mepipz)$_2$bpy]$_3$}$^{2+}$ complex ion was observed. The following alternative route started with {[(η^6-*p*-cymene)RuCl]$_2$(μ-Cl)$_2$}, which was prepared according to literature procedures.[48,49] A mixture of {[(η^6-*p*-cymene)RuCl]$_2$(μ-Cl)$_2$} (0.23 g, 0.00038 mol, 1 eq.) and dcbpy (0.19 g, 0.00076 mol, 2 eq.) in 80 mL DMF was heated to 65 °C for 4 h. Then excess (mepipz)$_2$bpy (0.60 g, 0.0017 mol, 4.5 eq.) was added and the reaction was refluxed for 4 additional hours, cooled to room temperature, and the solvent evaporated. The crude reaction mixture was dissolved in water, washed with methylene chloride (3 × 50 mL), and then metathesized to the hexafluorophosphate salt by adding $NaPF_6$ (0.015 mol, 20 eq.) dissolved in a minimum volume of water. The precipitate was isolated by filtration and was washed with water and then acetone to yield 0.35 g (70%) of **5**. ^{1}H-NMR (300 MHz; D_2O): δ 8.59 (s br, 2H), 7.84 (d, J = 5.5 Hz, 2H), 7.68 (d, J = 2.8 Hz, 2H), 7.63 (d, J = 2.7 Hz, 2H), 7.45 (d, J = 5.8 Hz, 2H), 7.21 (d, J = 6.6 Hz, 2H), 6.99 (d, J = 6.6 Hz, 2H), 6.68 (dd, J = 6.5, 1.1 Hz, 2H), 6.49 (dd, J = 5.3, 0.9 Hz, 2H), 4.24–3.96 (m, 8H), 3.58–3.37 (m, 8H), 3.38–3.14 (m, 8H), 3.13–2.93 (m, 8H), 2.80 (s, 6H), 2.78 (s, 6H). HR ESI-MS m/z (obs) 525.2150 (M^{2+}), m/z (calcd) 525.2139.

Deprotonation of compounds 1–6

Complexes **1–6** were dissolved in methanol to which a solution of aqueous tetramethylammonium hydroxide (10 equivalents) was added. The solution was stirred for 30 minutes at room temperature and concentrated causing the ruthenium complex to precipitate. The complexes were isolated by filtration and washed with water and dried under vacuum. The deprotonated dyes will be designated as **1-CO$_2^-$** to **6-CO$_2^-$**.

ZnO nanocrystal (NC) synthesis[16]

To a 0.1 M solution of $Zn(O_2CCH_3)_2{\cdot}2H_2O$ (25 mL, 2.51 mmol) in DMSO, a 0.55 M solution of $[NMe_4]OH{\cdot}5H_2O$ (7.73 mL, 4.25 mmol) in ethanol was added dropwise over the course of 30–180 s and allowed to stir at room temperature (*ca.* 24 °C) for up to 30 minutes. The longer reaction times led to larger particles. The diameters were determined using electronic absorption spectra.[39] To induce precipitation, an aliquot of the solution was removed and added to three times the volume of ethyl acetate. The turbid mixture was centrifuged using a LW Scientific Ultra-8 V centrifuge. After the liquid was decanted, the white pellet was dispersed in a minimum of ethanol and precipitated a second time. The purified ZnO NCs were mixed with methanol to yield an optically clear dispersion. To obtain a mass of ZnO, a known volume of the dispersion was evaporated and then heated to 500 °C in air for one hour to remove organics. Based on the initial mass of zinc acetate used a typical yield for the ZnO NC preparation was 78–80%.

Sample preparation: steady state absorption, emission and NMR

In all samples the amount of dye was held constant throughout the experiment and the amount of ZnO was varied in subsequent samples. In a typical experiment aliquots of 3.0×10^{-4} M ZnO nanocrystals (3.2 nm in diameter) dispersed in methanol were added to methanol solutions of dye (1.0×10^{-3} M) that had been deprotonated with ten equivalents of $[Me_4N][OH]$. The samples were then diluted to a total volume of 1.2 mL with methanol. Samples were allowed to equilibrate for 2 h before any measurements were taken. Methanol-d_4 was used for the NMR experiments.

Acknowledgements

This material is based upon work supported by the U.S. Department of Energy, Office of Science, Office of Basic Energy

Sciences under Award Number DE-FG02-07ER15913. This work was carried out in part using hardware and/or software provided by the University of Minnesota Supercomputing Institute.

References

1 A. Hagfeldt, G. Boschloo, L. C. Sun, L. Kloo and H. Pettersson, *Chem. Rev.*, 2010, **110**, 6595.
2 M. Gratzel, *Inorg. Chem.*, 2005, **44**, 6841.
3 S. Ardo and G. J. Meyer, *Chem. Soc. Rev.*, 2009, **38**, 115.
4 N. A. Anderson and T. Lian, *Annu. Rev. Phys. Chem.*, 2005, **56**, 491.
5 J. B. Asbury, R. J. Ellingson, H. N. Ghosh, S. Ferrere, A. J. Nozik and T. Lian, *J. Phys. Chem. B*, 1999, **103**, 3110.
6 G. Ramakrishna, D. A. Jose, D. K. Kumar, A. Das, D. K. Palit and H. N. Ghosh, *J. Phys. Chem. B*, 2005, **109**, 15445.
7 D. Stockwell, Y. Yang, J. Huang, C. Anfuso, Z. Q. Huang and T. Q. Lian, *J. Phys. Chem. C*, 2010, **114**, 6560.
8 N. A. Anderson, X. Ai and T. Lian, *J. Phys. Chem. B*, 2003, **107**, 14414.
9 C. Bauer, G. Boschloo, E. Mukhtar and A. Hagfeldt, *J. Phys. Chem. B*, 2001, **105**, 5585.
10 G. Benko, J. Kallioinen, J. E. I. Korppi-Tommola, A. P. Yartsev and V. Sundstrom, *J. Am. Chem. Soc.*, 2002, **124**, 489.
11 R. W. Fessenden and P. V. Kamat, *J. Phys. Chem.*, 1995, **99**, 12902.
12 J. Kallioinen, G. Benko, P. Myllyperkio, L. Khriachtchev, B. Skarman, R. Wallenberg, M. Tuomikoski, J. Korppi-Tommola, V. Sundstrom and A. P. Yartsev, *J. Phys. Chem. B*, 2004, **108**, 6365.
13 R. Katoh, A. Furube, A. V. Barzykin, H. Arakawa and M. Tachiya, *Coord. Chem. Rev.*, 2004, **248**, 1195.
14 R. Katoh, A. Furube, K. Hara, S. Murata, H. Sugihara, H. Arakawa and M. Tachiya, *J. Phys. Chem. B*, 2002, **106**, 12957.
15 P. Kar, S. Verma, A. Das and H. N. Ghosh, *J. Phys. Chem. C*, 2009, **113**, 7970.
16 D. A. Schwartz, N. S. Norberg, Q. P. Nguyen, J. M. Parker and D. R. Gamelin, *J. Am. Chem. Soc.*, 2003, **125**, 13205.
17 A. S. Huss, A. Bierbaum, R. Chitta, D. J. Ceckanowicz, K. R. Mann, W. L. Gladfelter and D. A. Blank, *J. Am. Chem. Soc.*, 2010, **132**, 13963.
18 A. S. Huss, J. E. Rossini, D. J. Ceckanowicz, J. N. Bohnsack, K. R. Mann, W. L. Gladfelter and D. A. Blank, *J. Phys. Chem. C*, 2011, **115**, 2.
19 J. E. Rossini, A. S. Huss, J. N. Bohnsack, D. A. Blank, K. R. Mann and W. L. Gladfelter, *J. Phys. Chem. C*, 2011, **115**, 11.
20 O. Taratula, E. Galoppini, D. Wang, D. Chu, Z. Zhang, H. H. Chen, G. Saraf and Y. C. Lu, *J. Phys. Chem. B*, 2006, **110**, 6506.
21 M. J. Cook, A. P. Lewis, G. S. G. Mcauliffe, V. Skarda, A. J. Thomson, J. L. Glasper and D. J. Robbins, *J. Chem. Soc., Perkin Trans. 2*, 1984, 1293.
22 D. Martineau, M. Beley and P. C. Gros, *J. Org. Chem.*, 2006, **71**, 566.
23 S. Rau, T. Buttner, C. Temme, M. Ruben, H. Gorls, D. Walther, M. Duati, S. Fanni and J. G. Vos, *Inorg. Chem.*, 2000, **39**, 1621.
24 B. P. Sullivan, J. A. Baumann, T. J. Meyer, D. J. Salmon, H. Lehmann and A. Ludi, *J. Am. Chem. Soc.*, 1977, **99**, 7368.
25 C. Viala and C. Coudret, *Inorg. Chim. Acta*, 2006, **359**, 984.
26 A. Breivogel, S. Wooh, J. Dietrich, T. Y. Kim, Y. S. Kang, K. Char and K. Heinze, *Eur. J. Inorg. Chem.*, 2014, 2720.
27 P. J. Giordano, C. R. Bock, M. S. Wrighton, L. V. Interrante and R. F. X. Williams, *J. Am. Chem. Soc.*, 1977, **99**, 3187.
28 G. Wolfbauer, A. M. Bond, G. B. Deacon, D. R. MacFarlane and L. Spiccia, *J. Am. Chem. Soc.*, 2000, **122**, 130.
29 W. Henry, C. G. Coates, C. Brady, K. L. Ronayne, P. Matousek, M. Towrie, S. W. Botchway, A. W. Parker, J. G. Vos, W. R. Browne and J. J. McGarvey, *J. Phys. Chem. A*, 2008, **112**, 4537.
30 V. Skarda, M. J. Cook, A. P. Lewis, G. S. G. Mcauliffe, A. J. Thomson and D. J. Robbins, *J. Chem. Soc., Perkin Trans. 2*, 1984, 1309.
31 P. J. Hore, *Nuclear Magnetic Resonance*, Oxford Univ. Press, 1995.
32 A. Badia, W. Gao, S. Singh, L. Demers, L. Cuccia and L. Reven, *Langmuir*, 1996, **12**, 1262.
33 O. Kohlmann, W. E. Steinmetz, X. A. Mao, W. P. Wuelfing, A. C. Templeton, R. W. Murray and C. S. Johnson, *J. Phys. Chem. B*, 2001, **105**, 8801.
34 B. S. Zelakiewicz, A. C. de Dios and Y. Y. Tong, *J. Am. Chem. Soc.*, 2003, **125**, 18.
35 R. Vatassery, J. A. Hinke, A. Sanchez-Diaz, R. Hue, K. R. Mann, D. A. Blank and W. L. Gladfelter, *J. Phys. Chem. C*, 2013, **117**, 10708.
36 C. M. Olsen, M. R. Waterland and D. F. Kelley, *J. Phys. Chem. B*, 2002, **106**, 6211.
37 H. Horiuchi, R. Katoh, K. Hara, M. Yanagida, S. Murata, H. Arakawa and M. Tachiya, *J. Phys. Chem. B*, 2003, **107**, 2570.
38 D. J. Norris, in *Nanocrystal Quantum Dots*, ed. V. I. Klimov, CRC Press, Boca Raton, Florida, 2nd edn, 2010, ch. 2, pp. 63–96.
39 R. Viswanatha, S. Sapra, B. Satpati, P. V. Satyam, B. N. Dev and D. D. Sarma, *J. Mater. Chem.*, 2004, **14**, 661.
40 S. Gutmann, M. Conrad, M. A. Wolak, M. M. Beerbom and R. Schlaf, *J. Appl. Phys.*, 2012, **111**, 123710.
41 G. Maerker and F. H. Case, *J. Am. Chem. Soc.*, 1958, **80**, 2745.
42 G. J. ten Brink, I. W. C. E. Arends, M. Hoogenraad, G. Verspui and R. A. Sheldon, *Adv. Synth. Catal.*, 2003, **345**, 497.
43 D. Zhang, J. P. Telo, C. Liao, S. E. Hightower and E. L. Clennan, *J. Phys. Chem. A*, 2007, **111**, 13567.

44 D. A. Freedman, T. P. Gill, A. M. Blough, R. S. Koefod and K. R. Mann, *Inorg. Chem.*, 1997, **36**, 95.
45 N. G. Connelly and W. E. Geiger, *Chem. Rev.*, 1996, **96**, 877.
46 M. J. T. Frisch, G. W. Trucks, H. B. Schlegel, G. E. Scuseria, M. A. Robb, J. R. Cheeseman, G. Scalmani, V. Barone, B. Mennucci, G. A. Petersson, H. Nakatsuji, M. Caricato, X. Li, H. P. Hratchian, A. F. Izmaylov, J. Bloino, G. Zheng, J. L. Sonnenberg, M. Hada, M. Ehara, K. Toyota, R. Fukuda, J. Hasegawa, M. Ishida, T. Nakajima, Y. Honda, O. Kitao, H. Nakai, T. Vreven, J. A. Montgomery Jr., J. E. Peralta, F. Ogliaro, M. Bearpark, J. J. Heyd, E. Brothers, K. N. Kudin, V. N. Staroverov, R. Kobayashi, J. Normand, K. Raghavachari, A. Rendell, J. C. Burant, S. S. Iyengar, J. Tomasi, M. Cossi, N. Rega, J. M. Millam, M. Klene, J. E. Knox, J. B. Cross, V. Bakken, C. Adamo, J. Jaramillo, R. Gomperts, R. E. Stratmann, O. Yazyev, A. J. Austin, R. Cammi, C. Pomelli, J. W. Ochterski, R. L. Martin, K. Morokuma, V. G. Zakrzewski, G. A. Voth, P. Salvador, J. J. Dannenberg, S. Dapprich, A. D. Daniels, Ö. Farkas, J. B. Foresman, J. V. Ortiz, J. Cioslowski and D. J. Fox, *Gaussian 09 (Revision A.1)*, Gaussian, Inc., Wallingford CT, 2009.
47 S. J. Slattery, N. Gokaldas, T. Mick and K. A. Goldsby, *Inorg. Chem.*, 1994, **33**, 3621.
48 E. Hodson and S. J. Simpson, *Polyhedron*, 2004, **23**, 2695.
49 M. K. Nazeeruddin, S. M. Zakeeruddin, J. J. Lagref, P. Liska, P. Comte, C. Barolo, G. Viscardi, K. Schenk and M. Graetzel, *Coord. Chem. Rev.*, 2004, **248**, 1317.